Title: Vascular self-healing within carbon fibre reinforced polymer stringer run-out configurations

Authors: R. Luterbacher, T.S. Coope, R.S. Trask, I.P. Bond

Keywords: FRP, bonded joints, self-healing, repair

Abstract

Stringer debonding within stiffened, assembled aerospace structures is one of the most critical damage scenarios that can occur in such structures. As a result, a degree of redundancy is inherently built-in to the design process of skin-stringer configurations to mitigate against premature and in-service failure. Introducing a "self-healing" solution for stringer run-out configurations has the benefit of mitigating and controlling damage initiation, and by introducing this concept there is great potential to reduce excessive conservative safety margins that could ultimately lead to more lightweight designs. Vascular self-healing technology has been successfully implemented into a simplified strap lap specimen, showing that the introduction of a vascular microchannel reduces the strength by 15% but has little effect on the stiffness. Upon delivery and cure of epoxy-based self-healing agents full recovery of the mechanical properties was observed. This self-healing approach has been further implemented into industrially relevant, larger stringer run-out panels as a feasibility study, in which no knockdown to mechanical properties caused by the embedded vascular microchannels has been observed, this study has also shown similar promising results in terms of performance recovery.

Introduction

The Achilles' heel of advanced fibre reinforced polymer composites generally centres around the matrix properties as these tend to have mechanical properties (e.g. modulus, strength) that are one or two orders of magnitude lower than the properties of the fibres. Even when small-scale damage manifests itself within the microstructure this does not typically lead to immediate load bearing loss of the structure, however, a reduction in mechanical performance is observed. A variety of strategies are currently used in order to prevent intra- and interlaminar matrix damage, such as the development of tougher resin systems, interleaves and the use of through thickness reinforcements [1].

A biomimetic approach in order to "heal" matrix damage - normally referred to as self-healing or autonomous repair - has been explored over the last 20 years. A variety of extensive literature reviews that detail previously investigated self-healing agents and test methods are available [2–4] and, therefore, a succinct summary of these activities is outlined in this section. Two different approaches to self-healing exists, namely (1) intrinsic and (2) extrinsic. The first approach relies on the innate properties of the polymer matrix material or embedded additives that can undergo reversible reactions. Examples include the use of Diels-Alder based matrix materials that exhibit a preferential rupture at a thermally reversible bond in the network [5,6] or the use of ethylmethylacrylic acid (EMAA) filaments that, upon heating, can be melted to rebond fracture surfaces [7,8]. In the second approach (i.e. extrinsic), a liquid healing agent can be encapsulated in the material via microcapsules or delivered via microchannels (referred to as vascules). Upon rupture of microcapsules or breach of microvascular channels, the liquid healing agent is delivered into the crack plane, where it can be made to polymerise into a structural solid. A variety of healing chemistries have been explored [9], which either rely on the reaction of the healing agent with a catalyst already embedded in the matrix [10], undergo localised mixing on the fracture plane [11,12], exploit single component healing chemistries [13] or utilise premixed healing agents [14]. Whereas the healing potential of intrinsic and microencapsulated healing agents is limited by their volume, larger damage regions can be addressed with the vascular approach as the healing agent can be delivered from a larger external reservoir [11,14].

The predominant aim of this research into self-healing advanced fibre reinforced polymers focuses on the demonstration of the healing capability following damage created under simple fracture type test configurations, i.e. Mode I and Mode II testing, or the recovery of low velocity impact damage. In both scenarios, the damage path is constrained and relatively large. In contrast, only a limited amount of research is found for more complex loading scenarios [15–17], even though promising results have been observed.

Skin-stiffened structures are widely used within lightweight applications such as aerospace. For a variety of reasons, such as access holes, geometric requirements or loading necessities, stringers have to be terminated within a wing structure or fuselage. These so called "stringer run-outs" are sensitive to localised damage initiation as the loads from the stringer end have to be transferred into the skin, leading to the need for localised design solutions [18] or the use of additional fasteners to assure fail safe design criteria can be met. Upon excessive loading, the stringer tends to delaminate at the skin-stringer interface and then delaminations propagate in the skin. This mechanism has been described and covered by several authors [19–22]. Manufacturing and testing of stringer run-out specimens is both time consuming and material intensive. However, a simpler specimen configuration (refer to Figure 1), called a compound joint [23] or strap-lap specimen [24], exhibits a similar damage mechanism as the more complex stringer run-out specimen.

The aim of this paper is to show the potential for using a vascular approach in a simplified strap-lap specimen to heal delaminations initiating at the tip of the flange and to transfer this knowledge and understanding to a large panel "stringer run-out" specimen.

Experimental

Strap lap specimens were manufactured from 200g/m^2, SE70 carbon/epoxy unidirectional pre-impregnated tape (Gurit, UK). The specimen nominal dimensions are shown in Figure 1. A quasi-isotropic lay-up ($[-45/90/45/0]_S$) was used for both the strap and the lap components. The strap was first vacuum bag cured under 1 atm at 100˚C for 100 minutes, with a ramp rate of 1˚C/min and then

machined to the desired dimensions. The lap was then co-bonded to the strap with the same curing schedule as the strap using a caul plate in the unstiffened region in order to prevent ply wrinkling and the creation of a resin pocket at the tip of the strap. No additional adhesive film was used and the strap was abraded with 500 SiC grit paper as preparation for bonding.

For the specimens containing vascules, the manufacturing route B described by Norris et al [25] was followed. Small local regions of specific plies, where vascules were to be positioned, were removed and PTFE coated NiCr wires (diameter 0.5 mm) were placed between these cut outs. The vascules protruded 10 mm from the tip of the lap to permit access in order to simulate future in-service applications as shown in Figure 1 (i) and (iii). In real skin-stiffener examples, the stiffening element length can be in the range of meters. However, the most probable delamination initiation point occurs at the tip of the flange and, therefore, the need for a vascular arrangement to deliver healing agent is very localised. The wire preforms were manually removed after curing.

After the curing process, end tabs were secondary bonded using Araldite 2015 (cured for 1 hour at 70˚C) to the lap, then the specimens were cut to the nominal dimensions, as shown in Figure 1 (i).

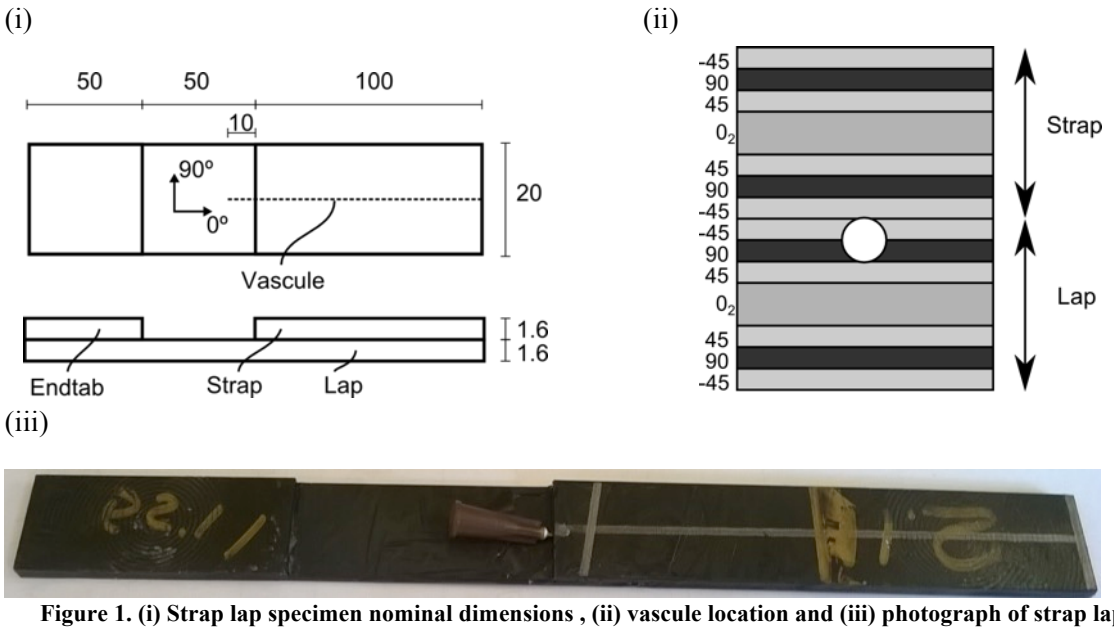

Figure 1. (i) Strap lap specimen nominal dimensions , (ii) vascule location and (iii) photograph of strap lap specimen with inserted needle for infusion in the protruding vascule. This protrusion simulates a potential later access point for the delivery of healing agent.

The stringer run-out specimens were manufactured following the process described by Trask et al. [26]. Specimen details are shown in Figure 2. Similar to the case for the strap lap specimen, the T-stringer was first laid up on a male aluminium mould as two L-sections and additional material was inserted in order to fill the deltoid. The manufacturing process is shown in Figure 2 (iii). The stringer foot had the same lay-up as the strap and was also manufactured from SE70 carbon/epoxy unidirectional tape (Gurit, UK) with an additional dwell of 2 hours in order to permit heating of the tooling. The stringer was machined to size and co-cured to the skin ($[-45/90/45/0]_S$) as was for the case of the strap lap specimen. A 5 mm long PTFE starter film (15 μm thickness) was introduced at the tip of the stringer-skin interface in order to promote failure along this interface. End tabs were secondary bonded with Araldite 2015 (cured for 1 hour at 70˚C) and specimens cut to the nominal dimensions as shown in Figure 2 (i) and (ii). Vascules were introduced into the skin as documented previously for the strap lap specimens, including a vascule protrusion of 10 mm from the tip of the flange. Additionally, one vascularised stringer run-out specimen without PTFE starter film was manufactured for fractographic observation.

The objective of this test was to qualitatively show the potential for self-healing within stringer run-out configurations and, therefore, only one baseline and one vascularised specimen were manufactured and tested.

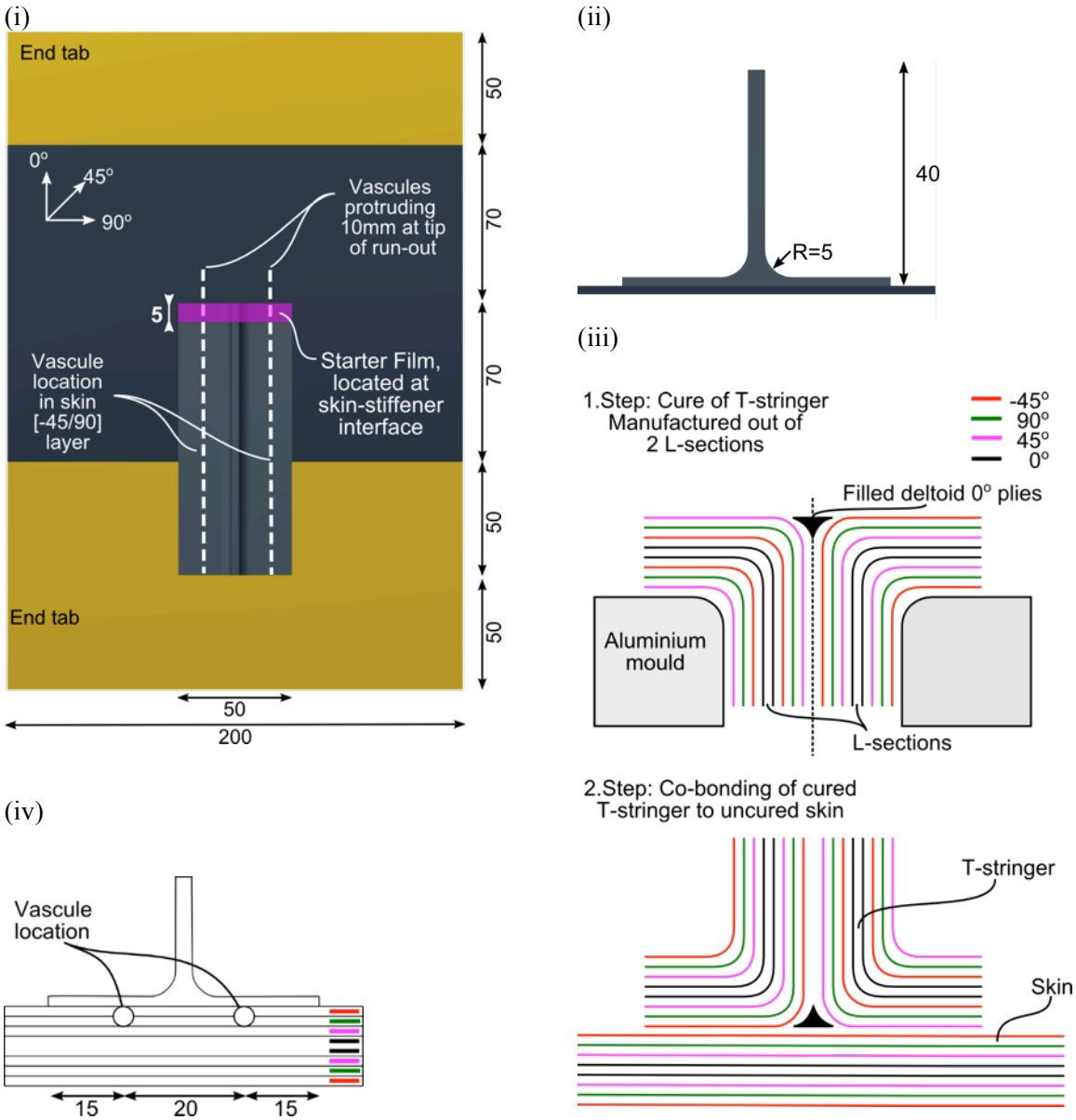

Figure 2. Stringer run-out specimen details. i) specimen dimensions, ii) stringer dimensions, iii) lay-up and manufacturing schema (Note that lay-up orientation refer to the skin of the stringer run out) and iv) vascule location.

Testing protocol

Strap lap specimens were tested under tensile loading on a universal testing machine (Schenck Hydropuls PSA) with a 75 kN calibrated load cell. Testing was performed at ambient temperature under displacement control of 2 mm/min. The stresses are calculated using the cross-section of the skin. The specimens were gripped 50 mm at either end leaving an initial grip-to-grip separation of 100 mm.

Two types of tests were performed (1) to determine the influence of the vascule on the mechanical properties and (2) to screen the healing behaviour. For the first test type, specimens were loaded until initiation of the delamination (Load L1 in Figure 3), unloaded and then loaded to failure (Load L2 in Figure 3). However, the second specimen type was tested until initiation of the delamination at the tip of the flange, which was visually observed and accompanied by a load drop. The specimens were then unloaded and loaded again to the delamination initiation threshold.

Two different healing agents were investigated: a commercially available, low viscosity epoxy resin (RT151, resin (RT151, Resintech, UK) and a bespoke in-house formulated toughened epoxy resin blend, further referred to as further referred to as THA. This blend is composed of 30pph of poly propylene diglycidyl ether, a reactive diluent, 20 reactive diluent, 20 pph of Hypox RA840 (a carboxyl-terminated butadiene acrylonitrile (CTBN) adducted Bisphenol adducted Bisphenol A diglycidyl ether (DGEBA) resin, commercially available from Hubron Speciality Ltd. (UK)) Speciality Ltd. (UK)) and 50 pph of Epon828 (DGEBA). The curing agent diethylenetriamine (DETA) was also used. (DETA) was also used. For further details on the healing chemistry of the toughened healing agent refer to Everitt et refer to Everitt et al. [27]. The curing cycle consisted of 1 hour at 65˚C in an oven for the RT151 healing agent and 1 healing agent and 1 hour at 45˚C followed by 3 hours at ambient temperature for the THA. The edges of the of the specimen were not sealed and no pressure was applied to the specimen during curing. The healing agents were healing agents were manually injected into the vascule using a syringe equipped with a 26 gauge needle. Figure 1 (iii) shows a strap lap specimen equipped with the 26 gauge needle prepared for infusion and

(i) (iii)

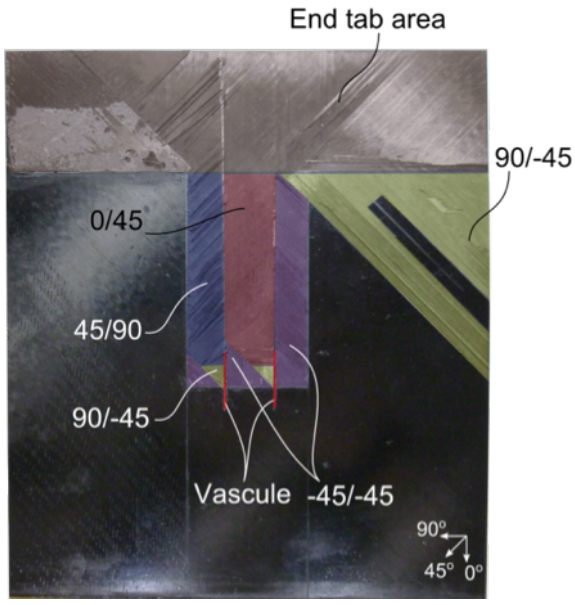

(ii)

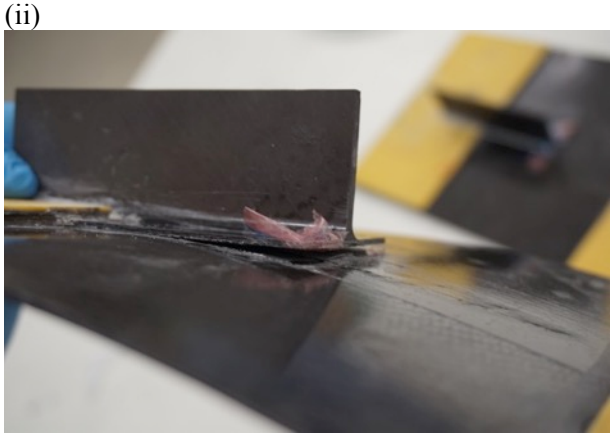

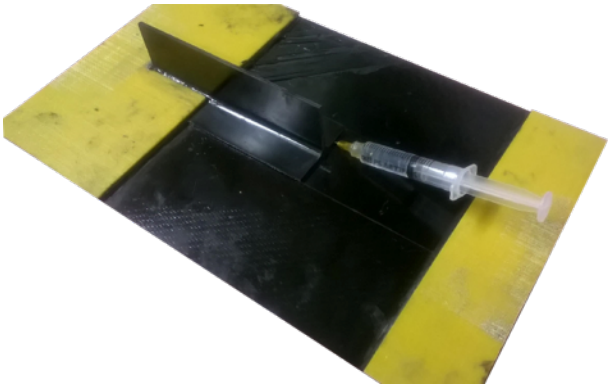

(iv)

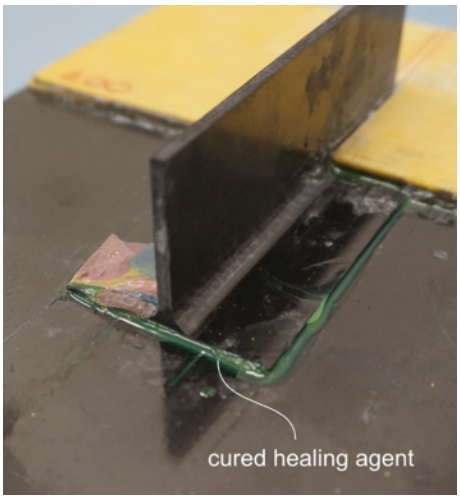

(i) the stringer run-out specimen during the injection process.

Two different healing efficiencies were calculated, the first relating to efficiency in the recovery of stiffness η_E and the second related to the recovery of the initial delamination strength η_σ, defined as follows;

$$\eta_E = \frac{E_{healed} - E_{damaged}}{E_{pristine} - E_{damaged}} \quad (1)$$

With

$$\eta_\sigma = \frac{\sigma_{INI\ healed}}{\sigma_{INI\ pristine}} \quad (2)$$

E_{healed}, $E_{damaged}$ and $E_{pristine}$ correspond to the stiffness in the healed, damaged and pristine state. $\sigma_{INI\ pristine}$ and $\sigma_{INI\ healed}$ correspond to the stress level at which the delamination initiated at the tip of the strap.

The apparent stiffness was calculated using the linear part of the measured stress-strain behaviour between 50 and 200 MPa, the strain level was calculated using the initial grip-to-grip distance and the stress level refers to the lap thickness. The pristine apparent stiffness $E_{pristine}$ was determined using the initial loading, the damaged apparent stiffness $E_{damaged}$ was determined during a second loading performed after delamination initiation and the healed apparent stiffness E_{healed} at the initial loading performed after injection and curing of the healing agent into the specimen.

The stringer run-out specimen was tested on a universal testing machine (Instron 1342) with a calibrated load cell of 250 kN under displacement control at a rate of 0.5 mm/min. The healing agent RT151 was used and the same healing procedure to that of the strap lap specimen was followed. The healing agent was doped (3 wt%) with a UV dye penetrant (Ardrox 9812) to aid visualisation.

Results and Discussion

Tensile tests

Figure 3 (i) shows representative stress-displacement curves and Table 1 summarises the test results.

Due to the offset between the loading axis and the neutral axis, the specimen deforms through the thickness as shown in Figure 3 (ii), causing through thickness stresses at the tip of the flange and delamination at the tip of the flange.

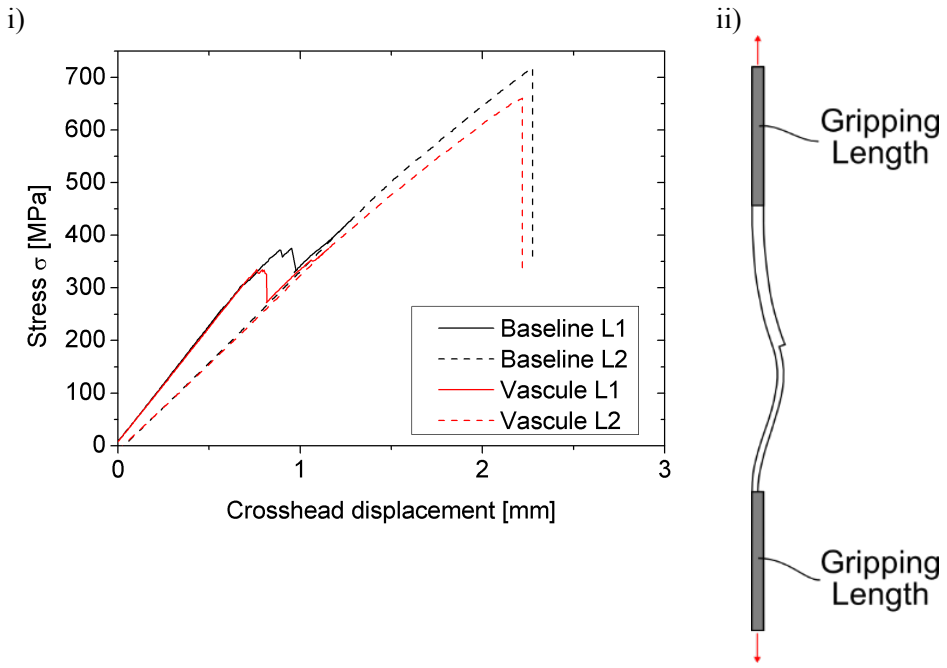

Figure 3. i) Representative stress-displacement curves for the baseline and the vascularised specimen and ii) Schematic out of plane deformation of the specimen.

Initially, the baseline and vascularised specimens behaved similarly and exhibited linear-elastic behaviour. A similar stiffness was observed, which was in accordance with observations made previously, in that small diameter vascules had little effect on the overall stiffness [28,29]. In the case studied, the vascule corresponded to approximately 0.6% of the cross section area of the lap without removing any plies oriented in the loading direction. However, the vascule did have an effect on the initiation load of the delamination with a reduction of 15%. This was due to the fact that the vascule acted as a free surface, as the -45 ˚ and 90˚ plies are terminated in order to accommodate the vascule. The damage initiation at the cut plies was observed on the fracture surface of the vascularised laminate in Figure 4. Upon damage the apparent stiffness was reduced by approximately 23% due to the delamination of the strap. The failure load of the strap lap specimen was reduced by 10% due to the introduction of the vascules.

Therefore, it can be stated that the embedded vascules had a modest effect on the mechanical properties and that a reduction in vascule diameter, such that it only affects one ply thickness, and alignment of the vascule with the local ply orientation may have further reduced this detrimental effect.

Table 1. Summary of test results for strap lap specimens. Effect of vascules on mechanical properties.

	Epristine [GPa]	**Edamaged [GPa]**	$\sigma_{INIpristine}$ **[MPa]**	**Strength UTS [MPa]**
Baseline	42.8 (1.6)	33.0 (1.0)	391 (21)	679 (40)
Vascularised	41.3 (1.4)	31.2 (0.9)	332(15)	608 (68)
Percentage change	-4%	-5%	-15%	-10%

Fractography

Figure 4 shows the fracture surfaces of the two types of strap lap specimen. In both cases, the damage initiated at the tip of the strap by ply splitting of the -45° and along the edge of the strap (marked as -45/-45 on the fracture surfaces, Figure 4). From this intralaminar damage, a delamination had initiated, which had propagated further inwards and downwards by ply splitting. This migration was due to the resolved tensile loading created by the mismatch between the load introduction and the neutral axis of the specimen. This migration continued until reaching the 0° ply oriented in the propagation direction, following a similar sequence described by Canturri et al.[30] under mixed mode loading. The delamination propagated further along this interface (marked as 0/45), with further fibre splitting, until reaching the grip area, where the delamination was arrested due to the applied gripping pressure. The main difference between the vascularised and baseline specimen was the fact that the vascule acted, as previously stated, as a free surface from which ply splitting and delaminations are initiated (refer to 90/-45 in Figure 4). Similar damage mechanisms have been observed by Greenhalgh et al [20] and Meeks et al [21] during testing of stringer run-out specimens.

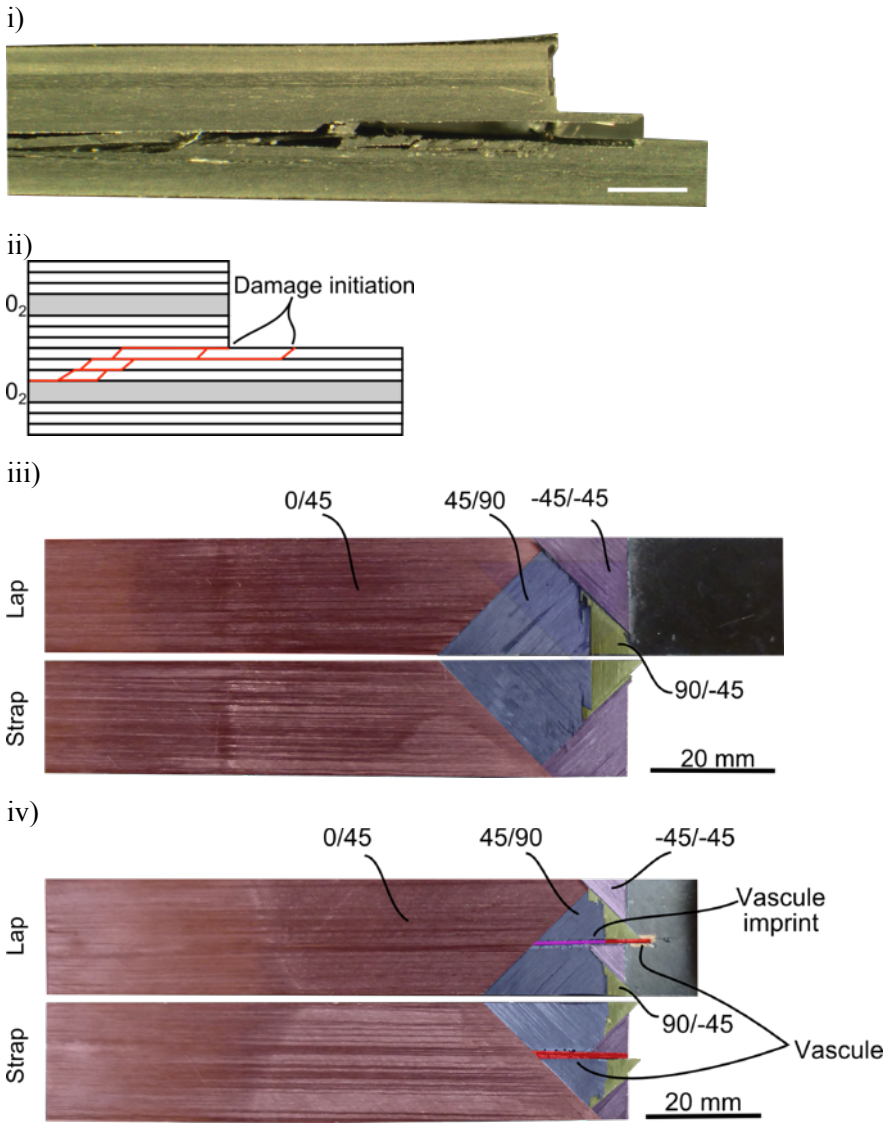

Figure 4. Damage surfaces i) Edge view, ii) Schematic of the edge view. Overhead view of the fracture surfaces for iii) the baseline and iv) vascularised specimen.

Healing efficiency

Figure 5 shows representative stress-displacement curves for the pristine and healed vascularised specimen and Table 2 summarises the healing results.

After healing, the stress-displacement response was similar to that of the pristine specimen with both healing agents successfully demonstrating a recovery in performance. The stiffness was fully recovered and the stress level at which the delaminations initiated was increased, leading to a healing efficiency, η_σ, ranging between 137-145%. It is expected that under fatigue loading the THA healed specimen will perform better due to its inherent toughness [29]. The reason for this increase in stress level at which the delaminations were initiated can be explained by the increase in the thickness of the resin rich interlayer (~350 μm, Figure 6 (i)) leading to locally higher fracture toughness values [31]. Therefore, due to the fact that additional resin is injected into the crack plane, the thickness increases marginally. In addition, the RT151 resin has a brittle behaviour, whereas the THA is ductile and as healing efficiencies in the same order of magnitude are observed, the main mechanism is likely to be attributed to the increase of fracture toughness due to the thicker resin rich interlayer [31]. The damage propagated along a similar path as in the pristine case failing the healing agent in both cases in a cohesive way (Figure 6 (iii), (iv)).

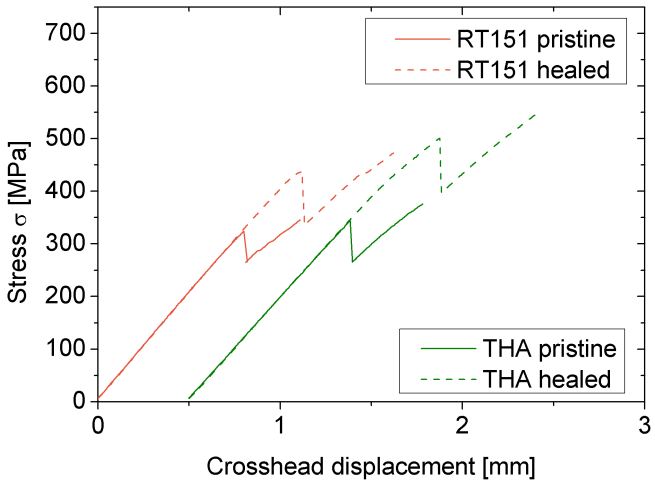

Figure 5. Representative healing curves for the strap lap specimen healed with RT151 and THA. Curves are off-set for improved visualisation

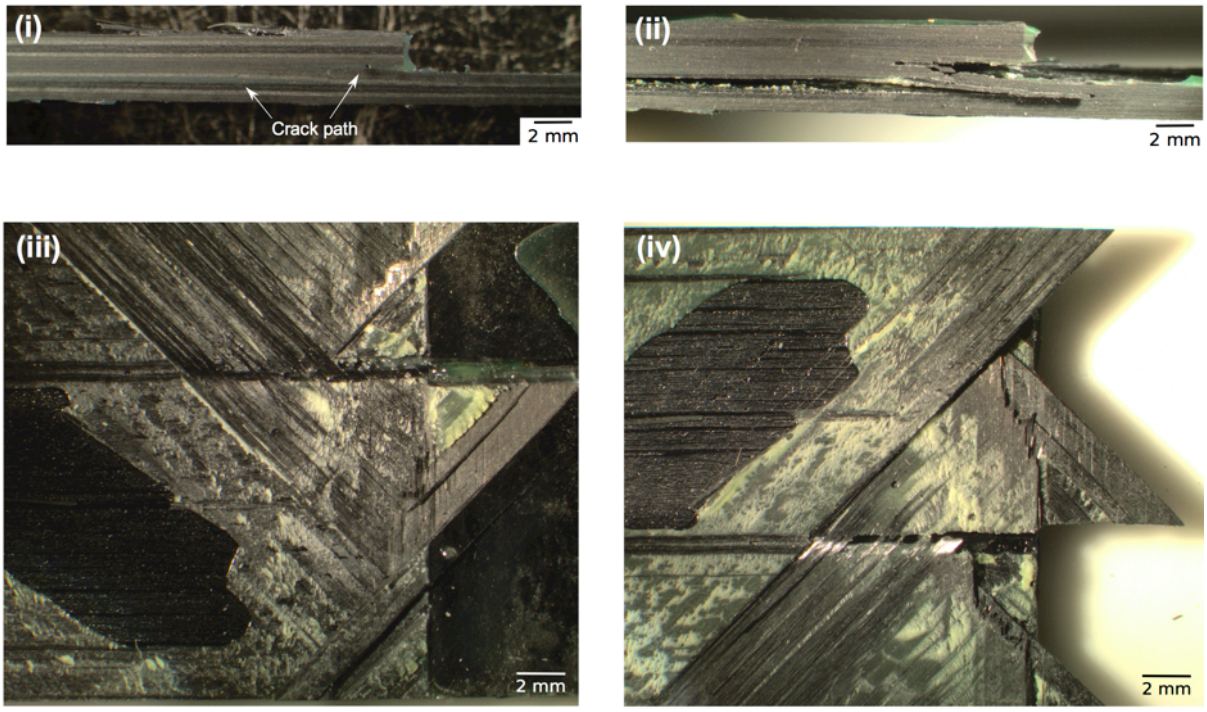

Figure 6 (i) Edge view of the healed RT151 strap lap specimen, (ii) edge view of the retested healed RT151 strap, (iii) microscopic investigation of the healed RT151 lap fracture plane, (iv) microscopic investigation of the healed RT151 strap fracture plane.

Table 2. Summary of healing results for the strap lap specimen healed with the two healing agents

	$E_{pristine}$ [GPa]	$E_{damaged}$ [GPa]	$\sigma_{INI\ pristine}$ [MPa]	E_{healed} [GPa]	$\sigma_{INI\ healed}$ [MPa]	η_E [%]	η_D [%]
RT151	41.0 (0.4)	31.6 (0.5)	324 (7)	40.8 (0.4)	445 (35)	98	137
THA	40.1 (0.9)	30.3 (0.6)	343 (16)	40.0 (0.4)	497 (40)	99	145

Stringer run-out self-healing demonstrator

Figure 7 (i) shows the load-displacement curves comparing the baseline and vascularised specimen and Figure 7 (ii) the pristine and healed vascularised specimen. For the non-healed, the specimens were loaded until approximately 125 kN, whereas the healed vascularised specimen was tested to failure. Prior to healing, the delamination in the vascularised specimen propagated until the

gripping area, where it was arrested due to the through thickness compressive stresses. Final failure of the healed vascularised specimen was tensile failure of the skin in the tip region of the stringer, after which the stringer had fully delaminated to the grip region, similar to the one observed for the baseline configuration

In contrast to the lap strap specimen, where the debonding of the strap occurred immediately (refer to Figure 3 (i)), a more progressive damage was observed for the stringer run-out specimen. Damage progression was only observed visually during testing, however, the following observations were noted. For the baseline and vascularised specimen (Figure 7 (i)) at ca. 60 kN the initial debonding of the stringer was observed. However, the load bearing behaviour of the vascularised specimen was higher (up to 7%) than for the baseline configuration. Therefore, one potential interpretation could be that the vascules acted as delamination arrestors. As only one specimen was tested no definitive conclusion can be drawn as to whether the improved behaviour of the vascularised specimen was due to material and manufacturing variability or if the vascules acted as delamination arrestors, thereby effectively compartmentalising the propagating debonding damage [25]

Within Figure 8 (i), the fracture surface of the vascularised specimen without PTFE release film is shown. No PTFE film was used in order to be able to compare the fracture surface with that of the comparable strap lap specimen (Figure 4). Due to the fact that similar fracture surfaces were observed, it could be concluded that a similar damage mechanism was present for both configurations. Similar to the case of the strap-lap specimen the damage initiates at the tip of the stringer foot at the cut plies that accommodates the vascules. The damage then propagates inwards and downwards as described by Greenhalgh et al [20] and Meeks et al [21]. However, in contrast to the strap lap specimen, the cut plies do not seem to have an effect on the damage initiation load.

Figure 8 (ii) shows the debonding from the stringer and skin. The vascularised specimen was then healed (Figure 8 (iii)) and the healing agent remained constrained to the debonded region (Figure 8 (iii)).

From the load-displacement curve (Figure 7 (ii)), a similar response was observed for both the initial and vascularised specimens. However, it was not possible to define a healing efficiency as the stiffness of the damaged specimen was not determined.

Nevertheless, it can be concluded that promising results were observed in terms of recovery in the disbond at the tip of the stringer run-out configuration. Future work will focus on a systematic approach in order to define a sensing – healing system which can autonomously trigger the healing event, similar to the examples in [14,16]. Tip delamination could be determined using a commercially available Structural Health Monitoring (SHM) technique, such as an ultrasonic transducer inducing Lamb waves for damage detection [32]. Upon damage detection, a healing agent could be delivered and locally activated in order to cure. The same SHM sensor could then be used to validate the healing event and assure the ongoing performance of the healed stringer run-out. Additional work will focus on the optimisation of the location of the vascules in order to mitigate the knockdown on the mechanical performance. Shorter, smaller, embedded or vascules oriented in ply directions are expected to reduce the impact of the vascules on the mechanical performance. In this way, the robustness and reliability of FRP structures could be improved thereby reducing the need for time consuming and expensive manual inspection and repair processes.

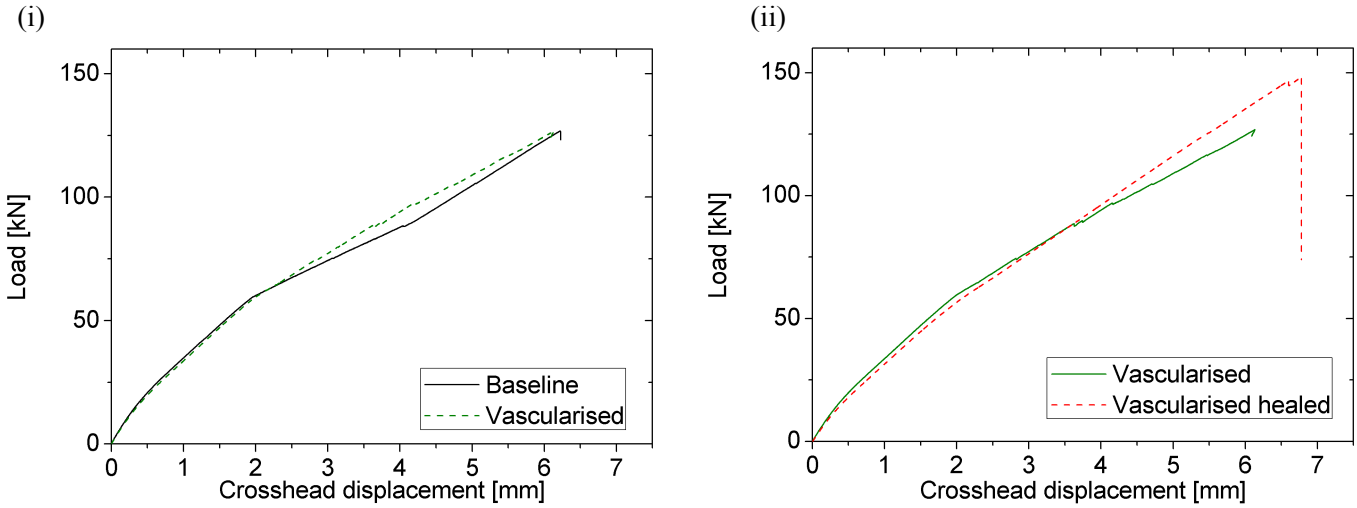

Figure 7 Comparision of load displacement curves for the i) baseline and vascularised stringer run-out specimen and ii) the pristine and healed loading of the vascularised stringer run-out specimen

(i)

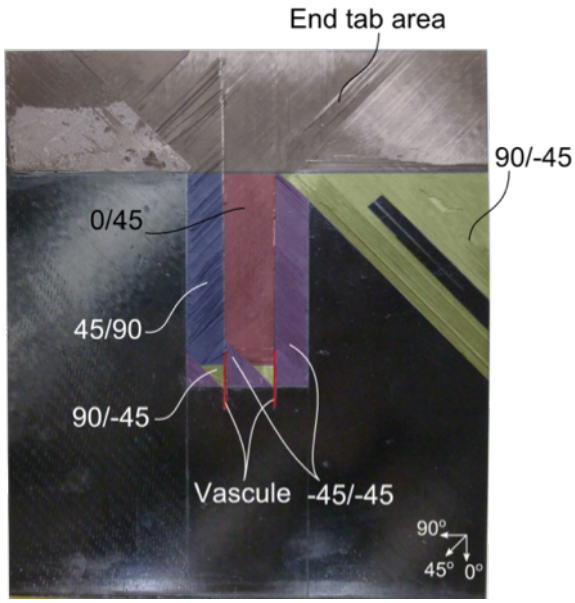

(ii)

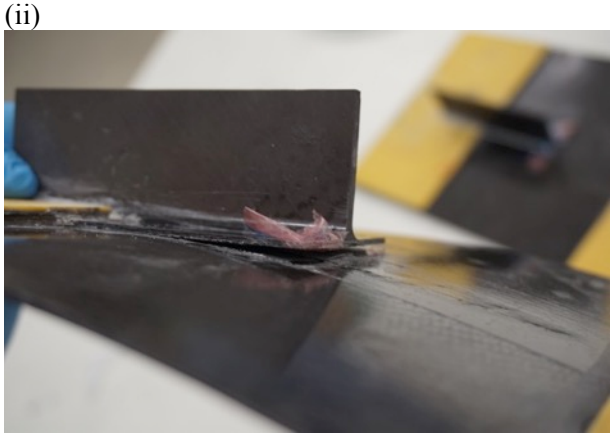

(iii)

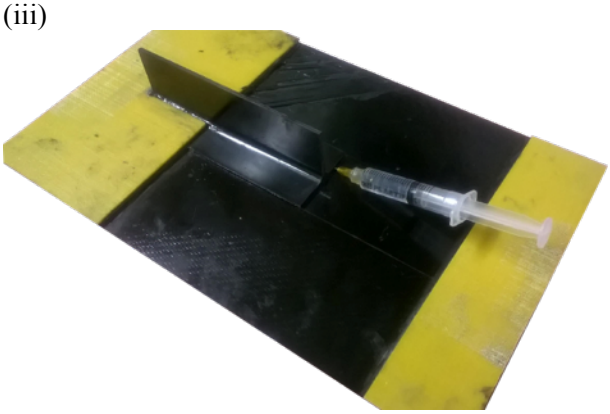

(iv)

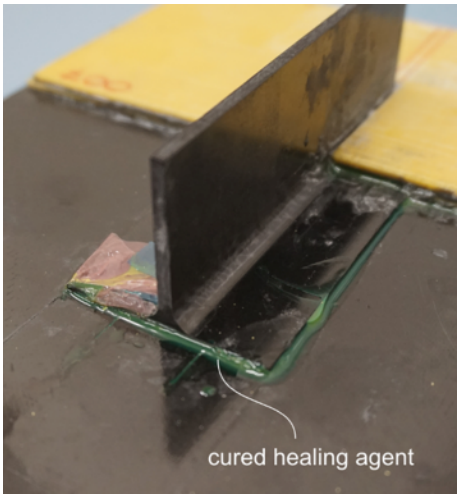

Figure 8 (i) Shows the fracture surface of a unhealed vascularised specimen, (ii) disbonding between the skin and the stringer, (iii) resin injection for healing into the protruding vascule. This protrusion simulates a potential later access point for delivery of the healing agent, and (vi) healing agent in the stringer run-out specimen

Conclusions

Stringer run-out damage mechanisms have been simulated using a small scale, strap lap specimen in order to assess the potential for self-healing using an in-situ vascular network. The introduction of a non-optimised vascular network (in terms of location and orientation) had marginal influence on the global mechanical properties: a reduction of approximately 15% in initial debonding strength and 10% in final failure load. By reducing the diameter of the vascule, changing its position or locally aligning with the host ply, there is scope to further reduce, or eliminate, the network's effect on the mechanical performance. In terms of property recovery, the initial stiffness was fully restored and the strength, in terms of initial disbonding, was increased due to the localised improvement in fracture toughness.

In order to demonstrate the potential to transfer these findings to larger, more realistic composite assemblies, two stringer run-out panels were manufactured, one as an unmodified baseline and another containing a vascular network. Both configurations behaved similarly and effective healing was observed. A similar damage pattern was observed as found for the simpler strap lap specimen, thus it can be surmised that a similar magnitude of healing recovery could be achieved. Future work will focus on optimising the vascular approach for the stringer run-out assembly, and consideration given as to how an autonomous sensing-healing system could be incorporated to increase the reliability and robustness of this technology and drive it towards industrial exploitation.

Acknowledgments

The authors would like to thank the UK Engineering and Physical Sciences Research Council (EPSRC) (EP/G036772), Fundació Obra Social la Caixa and the European FP7 HIPOCRATES (ACP3-GA-2013-605412) for funding this project.

References

[1] Greenhalgh E, Hiley M. The assessment of novel materials and processes for the impact tolerant design of stiffened composite aerospace structures. Compos Part A Appl Sci Manuf 2003;34:151–61.

[2] Blaiszik BJ, Kramer SLB, Olugebefola SC, Moore JS, Sottos NR, White SR. Self-Healing Polymers and Composites. Annu Rev Mater Res 2010;40:179–211.

[3] van der Zwaag S, Grande AM, Post W, Garcia SJ, Bor TC. Review of current strategies to induce self-healing behaviour in fibre reinforced polymer based composites. Mater Sci Technol 2014;30:1633–41.

[4] Diesendruck CE, Sottos NR, Moore JS, White SR. Biomimetic Self-Healing. Angew Chemie Int Ed 2015;54:10428–47.

[5] Nielsen C, Nemat-Nasser S. Crack healing in cross-ply composites observed by dynamic mechanical analysis. J Mech Phys Solids 2015;76:193–207.

[6] Turkenburg DH, Fischer HR. Diels-Alder based, thermo-reversible cross-linked epoxies for use in self-healing composites. Polymer (Guildf) 2015;79:187–94.

[7] Pingkarawat K, Wang CH, Varley RJ, Mouritz AP. Self-healing of delamination cracks in mendable epoxy matrix laminates using poly[ethylene-co-(methacrylic acid)] thermoplastic. Compos Part A Appl Sci Manuf 2012;43:1301–7.

[8] Yang T, Zhang J, Mouritz AP, Wang CH. Healing of carbon fibre–epoxy composite T-joints using mendable polymer fibre stitching. Compos Part B Eng 2013;45:1499–507.

[9] Hillewaere XKD, Du Prez FE. Fifteen chemistries for autonomous external self-healing polymers and composites. Prog Polym Sci 2015;49-50:121–53.

[10] Coope TS, Wass DF, Trask RS, Bond IP. Metal Triflates as Catalytic Curing Agents in Self-Healing Fibre Reinforced Polymer Composite Materials. Macromol Mater Eng 2014;299:208–18.

[11] Patrick JF, Hart KR, Krull BP, Diesendruck CE, Moore JS, White SR, et al. Continuous Self-Healing Life Cycle in Vascularized Structural Composites. Adv Mater 2014;26:4302–8.

[12] Ghazali H, Ye L, Zhang MQ. Interlaminar fracture of CF/EP composite containing a dual-component microencapsulated self-healant. Compos Part A Appl Sci Manuf 2016;82:226–34.

[13] Fifo O, Ryan K, Basu B. Glass fibre polyester composite with in vivo vascular channel for use in self-healing. Smart Mater Struct 2014;23:095017.

[14] Norris CJ, White JAP, McCombe G, Chatterjee P, Bond IP, Trask RS. Autonomous stimulus triggered self-healing in smart structural composites. Smart Mater Struct 2012;21:094027.

[15] Wang CH, Sidhu K, Yang T, Zhang J, Shanks R. Interlayer self-healing and toughening of carbon fibre/epoxy composites using copolymer films. Compos Part A Appl Sci Manuf 2012;43:512–8.

[16] Minakuchi S, Sun D, Takeda N. Hierarchical system for autonomous sensing-healing of

delamination in large-scale composite structures. Smart Mater Struct 2014;23:115014.

[17] Sakurayama N, Minakuchi S, Takeda N. Sensing and healing of disbond in composite stiffened panel using hierarchical system. Compos Struct 2015;132:833–41.

[18] Psarras S, Pinho ST, Falzon BG. Investigating the use of compliant webs in the damage-tolerant design of stiffener run-outs. Compos Part B Eng 2013;45:70–7.

[19] Minguet PJ, O'Brien TK. Analysis of Test Methods for characterizing skin/stringer debonding failures in reinforced composite panels. Compos. Mater. Test. Des. (Twelfth Vol., 1996, p. 105–24.

[20] Greenhalgh E, Garcia MH. Fracture mechanisms and failure processes at stiffener run-outs in polymer matrix composite stiffened elements. Compos Part A Appl Sci Manuf 2004;35:1447–58.

[21] Meeks C, Greenhalgh E, Falzon BG. Stiffener debonding mechanisms in post-buckled CFRP aerospace panels. Compos Part A Appl Sci Manuf 2005;36:934–46.

[22] Krueger R, Cvitkovich MK, O'Brien TK, Minguet PJ. Testing and Analysis of Composite Skin/Stringer Debonding under Multi-Axial Loading. J Compos Mater 2000;34:1263–300.

[23] Imperiale VA, Cosentino E, Weaver PM, Bond IP. Compound joint: A novel design principle to improve strain allowables of FRP composite stringer run-outs. Compos Part A Appl Sci Manuf 2010;41:521–31.

[24] Ashcroft IA, Wahab MMA, Crocombe AD, Hughes DJ, Shaw SJ. The effect of environment on the fatigue of bonded composite joints. Part 1: testing and fractography. Compos Part A Appl Sci Manuf 2001;32:45–58.

[25] Norris CJ, Bond IP, Trask RS. Interactions between propagating cracks and bioinspired self-healing vascules embedded in glass fibre reinforced composites. Compos Sci Technol 2011;71:847–53.

[26] Trask RS, Hallett SR, Helenon FMM, Wisnom MR. Influence of process induced defects on the failure of composite T-joint specimens. Compos Part A Appl Sci Manuf 2012;43:748–57.

[27] Everitt DT, Luterbacher R, Coope TS, Trask RS, Wass DF, Bond IP. Optimisation of epoxy blends for use in extrinsic self-healing fibre-reinforced composites. Polymer (Guildf) 2015;69:283–92.

[28] Kousourakis A, Bannister MK, Mouritz AP. Tensile and compressive properties of polymer laminates containing internal sensor cavities. Compos Part A Appl Sci Manuf 2008;39:1394–403.

[29] Luterbacher R, Trask RS, Bond IP. Static and fatigue tensile properties of cross-ply laminates containing vascules for self-healing applications. Smart Mater Struct 2016;25:015003.

[30] Canturri C, Greenhalgh ES, Pinho ST, Ankersen J. Delamination growth directionality and the subsequent migration processes – The key to damage tolerant design. Compos Part A Appl Sci Manuf 2013;54:79–87.

[31] Sela N, Ishai O, Banks-Sills L. The effect of adhesive thickness on interlaminar fracture

toughness of interleaved CFRP specimens. Composites 1989;20:257–64.

[32] Lee J-R, Takatsubo J, Toyama N. Disbond monitoring at wing stringer tip based on built-in ultrasonic transducers and a pulsed laser. Smart Mater Struct 2007;16:1025–35.